energies

MDPI

Article

Applications of Haar Wavelet-Finite Difference Hybrid Method and Its Convergence for Hyperbolic Nonlinear Schrödinger Equation with Energy and Mass Conversion

Xuan Liu [1], Muhammad Ahsan [2], Masood Ahmad [3], Muhammad Nisar [4,5], Xiaoling Liu [1,*], Imtiaz Ahmad [2] and Hijaz Ahmad [6,7]

1 Department of Mathematics, Hanshan Normal University, Chaozhou 515041, China; czliuxuan@126.com
2 Department of Mathematics, University of Swabi, Swabi 23200, Pakistan; ahsankog@uoswabi.edu.pk (M.A.); imtiazkakakhil@gmail.com (I.A.)
3 Department of Basic Sciences, University of Engineering and Technology Peshawar, Peshawar 25000, Pakistan; masoodsuf@gmail.com
4 Department of Mathematics and Statistics, Macquarie University, Sydney, NSW 2109, Australia; m.nisar666@gmail.com
5 Department of Mathematics, FATA University, Darra Adam Khel 26100, Pakistan
6 Department of Computer Engineering, Biruni University, Istanbul 34025, Turkey; hijaz555@gmail.com
7 Section of Mathematics, International Telematic University Uninettuno, Corso Vittorio Emanuele II, 39, 00186 Roma, Italy
* Correspondence: liuxiaoling@hstc.edu.cn

Citation: Liu, X.; Ahsan, M.; Ahmad, M.; Nisar, M.; Liu, X.; Ahmad, I.; Ahmad, H. Applications of Haar Wavelet-Finite Difference Hybrid Method and Its Convergence for Hyperbolic Nonlinear Schrödinger Equation with Energy and Mass Conversion. *Energies* **2021**, *14*, 7831. https://doi.org/10.3390/en14237831

Academic Editor: Federico Milano

Received: 4 October 2021
Accepted: 11 November 2021
Published: 23 November 2021

Abstract: This article is concerned with the numerical solution of nonlinear hyperbolic Schrödinger equations (NHSEs) via an efficient Haar wavelet collocation method (HWCM). The time derivative is approximated in the governing equations by the central difference scheme, while the space derivatives are replaced by finite Haar series, which transform it to full algebraic form. The experimental rate of convergence follows the theoretical statements of convergence and the conservation laws of energy and mass are also presented, which strengthens the proposed method to be convergent and conservative. The Haar wavelets based on numerical results for solitary wave shape of $|\varphi|$ are discussed in detail. The proposed approach provides a fast convergent approximation to the NHSEs. The reliability and efficiency of the method are illustrated by computing the maximum error norm and the experimental rate of convergence for different problems. Comparisons are performed with various existing methods in recent literature and better performance of the proposed method is shown in various tables and figures.

Keywords: conservative scheme; Haar wavelet; collocation method; Schrödinger equation

1. Introduction

The nonlinear hyperbolic Schrödinger equation govern most scientific and physical processes, and they play an essential role in nonlinear optics, Biomolecular dynamics, plasma physics, and water waves. Because finding the exact solution to these types of NHSEs is difficult due to the nonlinear term, numerical methods are an alternative method of determining their solution. In this paper, we considered the following NHSEs [1]

$$\frac{\partial^2\varphi}{\partial\tau^2}-\frac{\partial^2\varphi}{\partial s^2}+\mu_1\frac{\partial^2\varphi}{\partial\tau\partial s}-i\mu_2\frac{\partial\varphi}{\partial\tau}-i\mu_3\frac{\partial\varphi}{\partial s}+\mu_4\varphi+\mu_5|\varphi|^2\varphi=0,\quad a\le s\le b,\quad 0\le\tau\le T, \tag{1}$$

with the initial and boundary conditions

$$\varphi(s,0)=I_1(s),\quad \frac{\partial\varphi(s,0)}{\partial\tau}=I_2(s) \tag{2}$$

$$\varphi(a,\tau)=B_1(\tau),\quad \varphi(b,\tau)=B_2(\tau). \tag{3}$$

In the above equations I_1, I_2, B_1, and B_2 are known functions, $i^2 = -1$ and φ is the only unknown complex function, which is to be determined. The above NHSEs (1) have a lot of application in physics, such as Langmuir wave packet estimation in plasma physics [2], modeling of planar light bullets [3] and non-relativistic limit of the Klein-Gordon equation [4]. The two important properties of Equations (1)–(3) are the energy and mass conservation. The NHSEs (1)–(3) preserve the following expressions for total energy and total mass, which have been proved in [1]:

- Energy invariant

$$\mathcal{E}(\tau) := \int_a^b \left(\left| \frac{\partial \varphi}{\partial \tau} \right|^2 + \left| \frac{\partial \varphi}{\partial s} \right|^2 + i\mu_3 \varphi \overline{\frac{\partial \varphi}{\partial s}} + \mu_4 |\varphi|^2 + \frac{\mu_5}{2} |\varphi|^4 \right) ds = \mathcal{E}(0). \tag{4}$$

- Mass invariant

$$\mathcal{Q}(\tau) := \int_a^b \left[\left(\frac{\partial \varphi}{\partial \tau} \overline{\varphi} - \overline{\frac{\partial \varphi}{\partial \tau}} \varphi \right) - \mu_1 \varphi \overline{\frac{\partial \varphi}{\partial s}} - i\mu_2 |\varphi|^2 \right] ds = \mathcal{Q}(0). \tag{5}$$

Due to the above mentioned applications, different numerical techniques have been developed to solve the important NHSEs. These numerical technique are finite difference method [5–9], spline collocation methods [10] Galerkin method [11], Fourier pseudospectral method [12] and Multi-symplectic integrator [1]. The nonconservative scheme [5] may not handle the nonlinear blow up phenomena easily and the conservative schemes are presented to minimize these issues [7,9]. Some recent contributions are also reported in [13–15].

Recently, the research has been focused on the Haar wavelet application in the investigation and analysis of different problems in applied sciences. The different algorithms, based on weak and strong formulations, are the meshless wavelet method [16], the Daubechies wavelet-based method [17], the wavelet Galerkin method [18], and the wavelet collocation methods [19,20].A thorough introduction of the wavelets schemes for partial differential equations (PDEs) is given in [21]. Different scientific and engineering phenomena have been represented in the forms of ordinary differential equations (ODEs), integro-differential equations, and PDEs, which have been solved by Haar wavelets in the references [22–37]. A further development of the Haar wavelet is related to the solution of challenging fractional differential and integral equations [38–42]. The latest contribution on Haar wavelets is presented in [43] for the identification of software piracy.

The Haar wavelets have been used as an innovative and excellent mathematical tool for signal processing in physics and communication research [44] as well as in digital image/video processing and compression [45,46]. The Haar wavelet, like the finite difference approach, may convert PDEs into an algebraic system of equations, resulting in a well-conditioned number for the resulting system. This is the beauty of Haar wavelet in dealing with ill-conditioned problems in this way.

Haar wavelets based algorithms have also been reported to solve hyperbolic type PDEs. In [47], a linear hyperbolic PDE has been solved with Haar wavelet operational matrix method. In [48], the Haar wavelets were used to approximate the term $\frac{\partial^3 \varphi(s,\tau)}{\partial \tau \partial s^2}$ in order to get the numerical solution in the unit interval $[0, 1]$ using a transformation that converted the governing equation into system of PDEs. A Haar wavelet-finite difference hybrid method has been applied to the nonlinear parabolic Schrödinger equations in [20,49,50].

In this paper, the potential of the Haar wavelet is further applied to the NHSEs along with the theoretical convergence, which is supported by our numerical results in the interval $[a, b]$. Finite-difference and Haar wavelets are used to discretize the time and space derivatives, respectively. Because the Haar functions are discontinuous, the approximation begins with the highest order derivatives in the model equation. The unknown solution can be found by integrating the series further. A system of algebraic equations can be easily

solved by introducing these approximations in Equation (1). The next sections go into the details of the suggested method.

The paper is composed as follows. Section 2 is focused on the definitions of the Haar functions and their integrals. Section 3 presents the suggested numerical scheme. In Section 4, the convergence analysis is discussed. In Section 5, numerical findings are highlighted in details and in the last section, the concluding remarks are drawn.

2. Haar Functions

A generalized representation of the Haar functions is defined as

$$h_i(s) = \begin{cases} 1 & \text{for} \quad s \in [\zeta_1(i), \zeta_2(i)), \\ -1 & \text{for} \quad s \in [\zeta_2(i), \zeta_3(i)), \\ 0 & \text{elsewhere}, \end{cases} \tag{6}$$

where

$$\zeta_1(i) = a + \frac{(b-a)k}{m}, \quad \zeta_2(i) = a + \frac{(b-a)(k+0.5)}{m}, \quad \zeta_3(i) = a + \frac{(b-a)(k+1)}{m}.$$

Here $m = 2^j,\ j = 0, 1, \ldots,$ represents the level of the wavelet, $k = 0, 1, \ldots, m-1$ is the translation parameter, and $i = m + k + 1$. We note that $i \geq 2$. We define

$$h_1(s) = \begin{cases} 1 & \text{for} \quad s \in [a, b], \\ 0 & \text{elsewhere}, \end{cases}$$

which is also known as the mother wavelet. Due to the numerical estimation, we acknowledge a maximum estimation J of the entity j that expresses the level of the Haar wavelet in the earlier definition and J is then called the supreme level of resolution. We also introduced the integer $M = 2^J$. To keep the derivations simple, we intend to introduce some notations for the following integrals for $i = 2, 3, 4, \ldots$

$$p_{i,1}(s) = \int_a^s h_i(s')ds'$$
$$= \begin{cases} 0 & \text{for} \quad s < \zeta_1(i), \\ s - \zeta_1(i) & \text{for} \quad s \in [\zeta_1(i), \zeta_2(i)), \\ s - \zeta_1(i) - 2(s - \zeta_2(i)) & \text{for} \quad s \in [\zeta_2(i), \zeta_3(i)), \\ s - \zeta_1(i) - 2(s - \zeta_2(i)) + (s - \zeta_3(i)) & \text{for} \quad s \geq \zeta_3(i), \end{cases}$$

$$p_{i,2}(s) = \int_a^s p_{i,1}(s')ds'$$
$$= \begin{cases} 0 & \text{for} \quad s < \zeta_1(i), \\ \frac{1}{2}(s - \zeta_1(i))^2 & \text{for} \quad s \in [\zeta_1(i), \zeta_2(i)), \\ \frac{1}{2}[(s - \zeta_1(i))^2 - 2(s - \zeta_2(i))^2] & \text{for} \quad s \in [\zeta_2(i), \zeta_3(i)), \\ \frac{1}{2}[(s - \zeta_1(i))^2 - 2(s - \zeta_2(i))^2 + (s - \zeta_3(i))^2] & \text{for} \quad s \geq \zeta_3(i), \end{cases}$$

and

$$C = \int_a^b p_{i,1}(s')ds' = \frac{(b-a)^2}{4m^2} = \left(\frac{b-a}{2^{j+1}}\right)^2. \tag{7}$$

As $p_{i,1}(s)$ is increasing in the interval $[\zeta_1(i), \zeta_2(i))$ and decreasing in the interval $[\zeta_2(i), \zeta_3(i))$ but the maximum value is at $\zeta_2(i)$. Hence

$$\max_s(p_{i,1}(s)) = p_{i,1}(\zeta_2(i)) = \frac{b-a}{2m} = \frac{b-a}{2^{j+1}}. \tag{8}$$

It is worth noting that the following formula has been validated in [51]

$$\max_{s}(p_{i,2}(s)) = \frac{(b-a)^2}{4m^2} = \left(\frac{b-a}{2^{j+1}}\right)^2. \tag{9}$$

3. Haar Approximation

In this section, we consider Haar wavelets as a basic part of our numerical technique for spatial discretization. In order to construct the HWCM proposed in this paper, we consider the following form of Equation (1) [10]

$$\frac{\partial^2\varphi}{\partial\tau^2} - \frac{\partial^2\varphi}{\partial s^2} + \mathrm{i}\frac{\partial\varphi}{\partial\tau} + \lambda|\varphi|^2\varphi = 0, \tag{10}$$

where λ is constant. Due to discontinuity of the Haar functions, we start approximating the second order derivative with respect to s in Equation (10) by Haar functions as

$$\frac{\partial^2\varphi(s,\tau)}{\partial s^2} = \sum_{i=1}^{\infty}\lambda_i(\tau)h_i(s). \tag{11}$$

Integrating Equation (11) w.r.t s, from a to s,

$$\frac{\partial\varphi(s,\tau)}{\partial s} = \frac{\partial\varphi(a,\tau)}{\partial s} + \sum_{i=1}^{\infty}\lambda_i(\tau)p_{i,1}(s). \tag{12}$$

Integrating Equation (12) w.r.t s, from a to b,

$$\frac{\partial\varphi(a,\tau)}{\partial s} = \frac{\varphi(b,\tau)-\varphi(a,\tau)}{b-a} - \sum_{i=1}^{\infty}\lambda_i(\tau)\frac{C}{b-a}, \tag{13}$$

where C is given by Equation (7). By Equations (12) and (13), we obtain

$$\frac{\partial\varphi(s,\tau)}{\partial s} = \overline{w}_0(\tau) + \sum_{i=1}^{\infty}\lambda_i(\tau)\overline{h}_i(s), \tag{14}$$

where $\overline{w}_0(\tau) = \frac{\varphi(b,\tau)-\varphi(a,\tau)}{b-a}$ and $\overline{h}_i(s) = p_{i,1}(s) - \frac{C}{b-a}$. Again, by partially integrating Equation (14) w.r.t s, from a to s, we get

$$\varphi(s,\tau) = \widetilde{w}_0(s,\tau) + \sum_{i=1}^{\infty}\lambda_i(\tau)\widetilde{h}_i(s), \tag{15}$$

$$\text{where}\quad \widetilde{w}_0(s,\tau) = \varphi(a,\tau) + (s-a)\overline{w}_0(\tau),\quad \text{and}\quad \widetilde{h}_i(s) = (p_{i,2}(s) - (s-a)\frac{C}{b-a}. \tag{16}$$

If τ_{n-1} is the current time level, τ_n and τ_{n+1} is the consecutive next time levels, then using central difference approximation for time derivatives and introducing the following linearized θ-weighted scheme to Equation (10), we get

$$\begin{aligned}&\frac{\varphi(s,\tau_{n+1}) - 2\varphi(s,\tau_n) + \varphi(s,\tau_{n-1})}{\Delta\tau^2} - \theta\frac{\partial^2\varphi(s,\tau_{n+1})}{\partial s^2} - (1-\theta)\frac{\partial^2\varphi(s,\tau_n)}{\partial s^2}\\ &+\mathrm{i}\frac{\varphi(s,\tau_{n+1}) - \varphi(s,\tau_{n-1})}{2\Delta\tau} + \lambda|\varphi(s,\tau_n)|^2\left(\frac{\varphi(s,\tau_{n+1}) + \varphi(s,\tau_{n-1})}{2}\right) + \mathcal{O}(\Delta\tau^2) = 0.\end{aligned} \tag{17}$$

Using $\theta = 1$ in Equation (17), we get the well known implicit method to the NHSE

$$\frac{\varphi(s,\tau_{n+1})-2\varphi(s,\tau_n)+\varphi(s,\tau_{n-1})}{\Delta\tau^2}-\frac{\partial^2\varphi(s,\tau_{n+1})}{\partial s^2}+\mathrm{i}\frac{\varphi(s,\tau_{n+1})-\varphi(s,\tau_{n-1})}{2\Delta\tau}+\lambda|\varphi(s,\tau_n)|^2\left(\frac{\varphi(s,\tau_{n+1})+\varphi(s,\tau_{n-1})}{2}\right)+\mathcal{O}(\Delta\tau^2)=0. \tag{18}$$

To find the numerical solution based on the sum of finite Haar wavelet, we define

$$\varphi_M(s,\tau)=\widetilde{w}_0(s,\tau)+\sum_{i=1}^{2M}\lambda_i(\tau)\widetilde{h}_i(s). \tag{19}$$

Similarly, by intercepting the finite terms of Equations (11) and (14), we get

$$\begin{aligned}\frac{\partial\varphi_M(s,\tau)}{\partial s}&=\overline{w}_0(\tau)+\sum_{i=1}^{2M}\lambda_i(\tau)\overline{h}_i(s),\\ \frac{\partial^2\varphi_M(s,\tau)}{\partial s^2}&=\sum_{i=1}^{2M}\lambda_i(\tau)h_i(s).\end{aligned} \tag{20}$$

The relationship between exact and approximate representations are

$$\begin{aligned}&\varphi(s,\tau)=\varphi_M(s,\tau)+E_M(s,\tau),\ \text{ where }\ E_M(s,\tau)=\sum_{i=2M+1}^{\infty}\lambda_i(\tau)\widetilde{h}_i(s),\\ &\frac{\partial\varphi(s,\tau)}{\partial s}=\frac{\partial\varphi_M(s,\tau)}{\partial s}+\frac{\partial E_M(s,\tau)}{\partial s},\ \text{ where }\ \frac{\partial E_M(s,\tau)}{\partial s}=\sum_{i=2M+1}^{\infty}\lambda_i(\tau)\overline{h}_i(s),\end{aligned}$$

and

$$\frac{\partial^2\varphi(s,\tau)}{\partial s^2}=\frac{\partial^2\varphi_M(s,\tau)}{\partial s^2}+\frac{\partial^2E_M(s,\tau)}{\partial s^2},\ \text{ where }\ \frac{\partial^2E_M(s,\tau)}{\partial s^2}=\sum_{i=2M+1}^{\infty}\lambda_i(\tau)h_i(s).$$

The exact form of Equation (18) employing the Haar wavelet is now as follows

$$\frac{\varphi(s,\tau_{n+1})-2\varphi(s,\tau_n)+\varphi(s,\tau_{n-1})}{\Delta\tau^2}-\frac{\partial^2\varphi(s,\tau_{n+1})}{\partial s^2}+\mathrm{i}\frac{\varphi(s,\tau_{n+1})-\varphi(s,\tau_{n-1})}{2\Delta\tau}+\lambda|\varphi(s,\tau_n)|^2\left(\frac{\varphi(s,\tau_{n+1})+\varphi(s,\tau_{n-1})}{2}\right)=\mathcal{E}_{\mathcal{M}}^{\mathcal{H}}(s,\tau)+\mathcal{O}(\Delta\tau^2), \tag{21}$$

where $\mathcal{E}_{\mathcal{M}}^{\mathcal{H}}(s,\tau)$ is the Haar wavelet truncation error term, which is defined as

$$\begin{aligned}\mathcal{E}_{\mathcal{M}}^{\mathcal{H}}(s,\tau)=&-\frac{E_M(s,\tau_{n+1})-2E_M(s,\tau_n)+E_M(s,\tau_{n-1})}{\Delta\tau^2}\\ &+\frac{\partial^2E_M(s,\tau_{n+1})}{\partial s^2}-\mathrm{i}\frac{E_M(s,\tau_{n+1})-E_M(s,\tau_{n-1})}{2\Delta\tau}\\ &-\lambda|E_M(s,\tau_n)|^2\left(\frac{E_M(s,\tau_{n+1})+E_M(s,\tau_{n-1})}{2}\right).\end{aligned} \tag{22}$$

Dropping all the error terms $\mathcal{E}_{\mathcal{M}}^{\mathcal{H}}(s,\tau)+\mathcal{O}(\Delta\tau^2)$ and using the collocation points $s_l=a+(b-a)\frac{(l-0.5)}{2M}$, $l=1,2,\ldots,2M$, we have

$$\frac{\varphi(s_l,\tau_{n+1})-2\varphi(s_l,\tau_n)+\varphi(s_l,\tau_{n-1})}{\Delta\tau^2}-\frac{\partial^2\varphi(s_l,\tau_{n+1})}{\partial s^2}+\mathrm{i}\frac{\varphi(s_l,\tau_{n+1})-\varphi(s_l,\tau_{n-1})}{2\Delta\tau}+\lambda|\varphi(s_l,\tau_n)|^2\left(\frac{\varphi(s_l,\tau_{n+1})+\varphi(s_l,\tau_{n-1})}{2}\right)=0. \tag{23}$$

Now defining

$$\begin{aligned}\widetilde{\varphi}^{n}_{M,l} &:= \widetilde{w}_0(s_l,\tau_n) + \sum_{i=1}^{2M} \lambda_i^{M,n}\widetilde{h}_i(s_l),\\ \frac{\partial\widetilde{\varphi}^{n}_{M,l}}{\partial s} &:= \overline{w}_0(\tau_n) + \sum_{i=1}^{2M} \lambda_i^{M,n}\overline{h}_i(s_l),\\ \frac{\partial^2\widetilde{\varphi}^{n}_{M,l}}{\partial s^2} &:= \sum_{i=1}^{2M} \lambda_i^{M,n}h_i(s_l),\end{aligned} \tag{24}$$

we get

$$\frac{\widetilde{\varphi}^{n+1}_{M,l} - 2\widetilde{\varphi}^{n}_{M,l} + \widetilde{\varphi}^{n-1}_{M,l}}{\Delta\tau^2} - \frac{\partial^2\widetilde{\varphi}^{n+1}_{M,l}}{\partial s^2} + \mathrm{i}\frac{\widetilde{\varphi}^{n+1}_{M,l} - \widetilde{\varphi}^{n-1}_{M,l}}{2\Delta\tau} + \lambda\left|\widetilde{\varphi}^{n}_{M,l}\right|^2\left(\frac{\widetilde{\varphi}^{n+1}_{M,l} + \widetilde{\varphi}^{n-1}_{M,l}}{2}\right) = 0. \tag{25}$$

Putting Equation (24) in Equation (25), we get a system of $2M$ equations with $2M$ unknowns, which can be easily solved for λ_i's i.e.,

$$\begin{aligned}&\lambda_i^{M,n+1}\Big[\Big(1 + \frac{\mathrm{i}\Delta\tau}{2} + \frac{\lambda\Delta\tau^2}{2}\left|\widetilde{\varphi}^{n}_{M,l}\right|^2\Big)\widetilde{h}_i(s_l) - \Delta\tau^2 h_i(s_l)\Big]\\ &= 2\widetilde{\varphi}^{n}_{M,l} + \Big(\frac{\mathrm{i}\Delta\tau}{2} - \frac{\lambda\Delta\tau^2}{2}\left|\widetilde{\varphi}^{n}_{M,l}\right|^2 - 1\Big)\widetilde{\varphi}^{-}_{M,l}\Big(1 + \frac{\mathrm{i}\Delta\tau}{2} + \frac{\lambda\Delta\tau^2}{2}\left|\widetilde{\varphi}^{n}_{M,l}\right|^2\Big)\widetilde{w}_0(s_l,\tau_n).\end{aligned} \tag{26}$$

By using λ_i's in Equation (24), it is possible to obtain the desired numerical solution. To interpolate the solution at any point s, we define the formula below

$$\widetilde{\varphi}^{n+1}_{M}(s) := \widetilde{w}_0(s,\tau_{n+1}) + \sum_{i=1}^{2M} \lambda_i^{M,n+1}\widetilde{h}_i(s),$$

then $\widetilde{\varphi}^{n+1}_{M}(s) \approx \varphi(s,\tau_{n+1})$.

4. Convergence Analysis

This section is dedicated to the rate of convergence when $\varphi(s,\tau_P)$ is approximated by the numerical method described in Section 3. Let $0 = \tau_0 < \tau_1 < \ldots \tau_P = T$ be the partitioned of $[0,T]$ and P denotes a positive integer.

Theorem 1. *"Assume that* $\frac{\partial\varphi}{\partial\tau}$, $\frac{\partial^2\varphi}{\partial\tau^2}$, $\frac{\partial\varphi}{\partial s}$, $\frac{\partial^2\varphi}{\partial s^2}$, $\frac{\partial^3\varphi}{\partial s^3}$ *exist and are bounded in* $[a,b]\times[0,T]$. *For any* $M = 2^J$, $J = 0,1,2,\ldots,$ *and* $p = 0,1,\ldots P$, *where* P *is a positive integer, if* $\widetilde{\varphi}^{p}_{M}(s)$ *is the Haar wavelet solution and* $\varphi(s,\tau_p)$ *is the exact solution then*

$$\max_{0\le p\le P}\|\varphi(.,\tau_p) - \widetilde{\varphi}^{p}_{M}\|_{L_\infty(a,b)} \le \mathcal{O}(\frac{1}{M^2}) + \mathcal{O}(\Delta\tau^2), \text{ as } J\to\infty \text{ and } P\to\infty,$$

where $\Delta\tau = \max_{0\le p\le P-1}(\tau_{p+1} - \tau_p)$ *and* $L_\infty(a,b)$ *represents the infinity-norm in the interval (a,b)".*

Proof. For $p = 1,2,\ldots,P$ we have

$$\|\varphi(.,\tau_p) - \widetilde{\varphi}^{p}_{M}\|_{L_\infty(a,b)} \le \|E_M\|_{L_\infty(a,b)} + \|\varphi_M(.,\tau_p) - \widetilde{\varphi}^{p}_{M}\|_{L_\infty(a,b)},$$

where $\|E_M\|_{L_\infty(a,b)}$ is defined as

$$\|E_M\|_{L_\infty(a,b)} := \|\varphi(.,\tau_p) - \varphi_M(.,\tau_p)\|_{L_\infty(a,b)} = \max_s\left|\sum_{i=2M+1}^{\infty}\lambda_i\widetilde{h}_i(s)\right|.$$

It is shown in ([51] Equation (18)) that $\lambda_i \leq \beta/2^{j+1}$. In fact, it can be shown that $|\lambda_i| \leq \beta/2^{j+1}$ (which should also have been required in [51]). Therefore

$$\|E_M\|_{L_\infty(a,b)} \leq \beta \sum_{i=2M+1}^{\infty} \frac{1}{2^{j+1}} \max_s \left|\widetilde{h}_i(s)\right|. \tag{27}$$

By using successively Equation (16), the triangle inequality, Equations (7) and (9), we obtain

$$\begin{aligned}
\|E_M\|_{L_\infty(a,b)} &\leq \beta \sum_{i=2M+1}^{\infty} \frac{1}{2^{j+1}} \left[\max_s \left|(p_{i,2}(s)\right| + \max_s |(s-a)\frac{C}{b-a}\right|\right] \\
&\leq 2\beta(b-a)^2 \sum_{i=2M+1}^{\infty} \left(\frac{1}{2^{j+1}}\right)^3 \\
&\leq 2\beta(b-a)^2 \sum_{j=J+1}^{\infty} \sum_{k=0}^{2^j-1} \left(\frac{1}{2^{j+1}}\right)^3 \\
&= \beta(b-a)^2 \sum_{j=J+1}^{\infty} \left(\frac{1}{2^{j+1}}\right)^2 \\
&\leq \frac{\beta(b-a)^2}{3} \left(\frac{1}{2^{J+1}}\right)^2 = \mathcal{O}\left(\frac{1}{M^2}\right).
\end{aligned}$$

The second part $\|\varphi_M(.,\tau_p) - \widetilde{\varphi}_M^p\|_{L_\infty(a,b)}$ is the error due to the time iteration where we used central difference approximation, which is second order accurate in time, i.e., $\|\varphi_M(.,\tau_p) - \widetilde{\varphi}_M^p\| \leq \mathcal{O}(\Delta\tau^2)$. □

5. Test Cases

The HWCM is implemented by computing the results of various numerical test problems. We employed the second-order central difference for time discretization, and we generally want to expose the effect of spatial discretization by our results. The maximum error norms have been used for accuracy measurements, which are defined as;

$$\begin{aligned}
E_\infty &= \max_{1\leq l\leq 2M} |\varphi(s_l,\tau_P) - \widetilde{\varphi}_{M,l}^P|, \\
E_\infty^{Re} &= \max_{1\leq l\leq 2M} |\mathrm{Re}(\varphi(s_l,\tau_P)) - \mathrm{Re}(\widetilde{\varphi}_{M,l}^P)|, \\
E_\infty^{Im} &= \max_{1\leq l\leq 2M} |\mathrm{Im}(\varphi(s_l,\tau_P)) - \mathrm{Im}(\widetilde{\varphi}_{M,l}^P)|.
\end{aligned}$$

The important property in solving the NHSEs are the discrete conservation laws. To verify the HWCM we have calculated Equations (4) and (5) in the following way

$$\begin{aligned}
\mathcal{E}(\tau) :&= \int_a^b \left(\left|\frac{\partial\varphi}{\partial\tau}\right|^2 + \left|\frac{\partial\varphi}{\partial s}\right|^2 + \mathrm{i}\mu_3\varphi\overline{\frac{\partial\varphi}{\partial s}} + \mu_4|\varphi|^2 + \frac{\mu_5}{2}|\varphi|^4\right)ds \\
&\approx \frac{1}{2M}\sum_{i=0}^{2M}\left(|\mathcal{D}(s_i)|^2 + \left|\frac{\partial\widetilde{\varphi}_M^{n+1}(s_i)}{\partial s}\right|^2 + \mathrm{i}\mu_3\widetilde{\varphi}_M^{n+1}(s_i)\overline{\frac{\partial\widetilde{\varphi}_M^{n+1}(s_i)}{\partial s}}\right. \\
&\quad \left. + \mu_4\left|\widetilde{\varphi}_M^{n+1}(s_i)\right|^2 + \frac{\mu_5}{2}\left|\widetilde{\varphi}_M^{n+1}(s_i)\right|^4\right), \\
\mathcal{Q}(\tau) :&= \int_a^b \left[\left(\frac{\partial\varphi}{\partial\tau}\overline{\varphi} - \overline{\frac{\partial\varphi}{\partial\tau}}\varphi\right) - \mu_1\varphi\overline{\frac{\partial\varphi}{\partial s}} - \mathrm{i}\mu_2|\varphi|^2\right]ds \\
&\approx \frac{1}{2M}\sum_{i=0}^{2M}\left[\left(\mathcal{D}(s_i)\overline{\widetilde{\varphi}_M^{n+1}(s_i)} - \overline{\mathcal{D}(s_i)}\widetilde{\varphi}_M^{n+1}(s_i)\right) - \mu_1\widetilde{\varphi}_M^{n+1}(s_i)\overline{\frac{\partial\widetilde{\varphi}_M^{n+1}(s_i)}{\partial s}}\right. \\
&\quad \left. - \mathrm{i}\mu_2|\widetilde{\varphi}_M^{n+1}(s_i)|^2\right],
\end{aligned} \tag{28}$$

where $\mathcal{D}(s_i) = \frac{\widetilde{\varphi}_M^{n+1}(s_i) - \widetilde{\varphi}_M^{n-1}(s_i)}{2\Delta\tau}$.

Problem 1. *We consider the following linear form of Equation (1)*

$$\frac{\partial^2 \varphi}{\partial \tau^2} - \frac{\partial^2 \varphi}{\partial s^2} + \mathrm{i}\frac{\partial \varphi}{\partial \tau} + \varphi = 0, \quad 0 \le s \le 2\pi, \quad 0 \le \tau \le T.$$

with the initial conditions

$$\varphi(s,0) = e^{\mathrm{i}s}, \quad \frac{\partial \varphi(s,0)}{\partial \tau} = \mathrm{i}e^{\mathrm{i}s}$$

and boundary conditions

$$\varphi(0,\tau) = e^{\mathrm{i}\tau}, \quad \varphi(2\pi,\tau) = e^{\mathrm{i}(2\pi+\tau)}.$$

The exact solution is $\varphi(s,\tau) = e^{\mathrm{i}(s+\tau)}$.

The aim of presenting this linear case is to check and evaluate the accuracy, efficiency and the performance of this proposed Haar wavelet conservative scheme. In Table 1, to check the spatial convergence of the HWCM, we set $\Delta\tau = 0.0001$ *for various values of M. It was discovered that the theoretical and experimental rates of convergence for the space variable are in good agreement, and the CUP times demonstrate the program's efficiency and speed of calculation.*

Table 1. The numerical results at $\Delta\tau = 0.0001$, and $T = 1$ for Test Problem 1. Theoretical rate of convergence is 2 (see Theorem 1).

M	E_∞	Experimental Rate of Convergence	CPU Time (Second Unit)
1	1.3468×10^{-1}	-	0.5020
2	2.9363×10^{-2}	2.1975	1.2312
4	9.7614×10^{-3}	1.5888	2.4447
8	2.5647×10^{-3}	1.9283	6.9728
16	6.3987×10^{-4}	2.0029	13.2555

Problem 2. *We consider the following nonlinear type of Equation (1) [11]*

$$\frac{\partial^2 \varphi}{\partial \tau^2} - \frac{\partial^2 \varphi}{\partial s^2} + \mathrm{i}\frac{\partial \varphi}{\partial \tau} - 2|\varphi|^2\varphi = 0, \quad -50 \le s \le 50, \quad 0 \le \tau \le T.$$

The exact solution is

$$\varphi(s,\tau) = A\,\mathrm{sech}(Ks)e^{\mathrm{i}\Theta\tau},$$

where $A = |K|$ *and* $\Theta = \frac{1}{2}(-1 \pm \sqrt{1-4K^2})$. *The boundary and initial conditions can be obtained from the exact solution. In our calculations we have considered* $K = \frac{1}{4}$ *and* $\Theta = \frac{-1}{2} - \frac{\sqrt{3}}{4}$. *Further details can be found in [11].*

The reason we designed this example is to show the advantage of HWCM. To examine the error bounds, we analyzed the spatial and temporal discretization errors of the proposed method separately. To test the spatial convergence of the HWCM, we set $\Delta\tau = 0.0001$ *for various values of M and discovered that the theoretical and experimental rates of convergence for the space variable are in good agreement. To study the discretization error in time, we fixed M for different values of* $\Delta\tau$.

Problem 3. *Finally, consider the following form of NHSE*

$$\frac{\partial^2 \varphi}{\partial \tau^2} - \frac{\partial^2 \varphi}{\partial s^2} + \mathrm{i}\frac{\partial \varphi}{\partial \tau} + |\varphi|^2\varphi = 0, \quad -40 \le s \le 40, \quad 0 \le \tau \le T.$$

with the initial conditions

$$\varphi(s,0) = (1+\mathrm{i})se^{-10(1-s)^2}, \quad \frac{\partial \varphi(s,0)}{\partial \tau} = 0,$$

and homogeneous boundary conditions $\varphi(-40,\tau) = 0 = \varphi(40,\tau)$.

This problem is challenging due to the blow up phenomena of the soliton wave and has been considered in many papers as a practical problem [1,11,12] which has no exact solution. In Figure 3 the soliton wave is presented at different T, where the propagation of soliton is clearly seen as time increases. From this figure, one can examine that the soliton wave translates and converts into some lower waves quickly, and more ripples get up with the progression of wave. As the time $T \geq 5$*, the single soliton is split into more than one small solitons and moves violently. In Tables 2 and 3 the discrete conservation law are given for different T and* $\Delta\tau$ *by fixing M. From these table it can be easy to conclude that the HWCM can simulate the conservation of energy and mass in Equation (28) very well, respectively.*

Table 2. Conservation laws at various time levels with $M = 32$ and $\Delta\tau = 0.01$ for Test Problem 3.

T	$\mathcal{E}$	$\mathcal{Q}$
0.1	0.000463422189900	0.000519664924343i
0.2	0.000459011648589	0.000502983303627i
0.3	0.000450455456048	0.000479539412998i
0.4	0.000435697904302	0.000453609233561i
0.5	0.000413634348505	0.000429562779666i
0.6	0.000385022278416	0.000410899419094i
0.7	0.000352837966513	0.000399558520828i
0.8	0.000321889203778	0.000395661494238i
0.9	0.000297737255176	0.000397719510978i
1	0.000285221972077	0.000403216918935i

Table 3. Conservation laws at various time steps with $M = 8$ and $T = 1$ for Test Problem 3.

$\Delta\tau$	$\mathcal{E}$	$\mathcal{Q}$
0.005	0.000000000065664	0.00000000094289i
0.001	0.000000000065723	0.00000000094345i
0.0005	0.000000000065730	0.00000000094353i
0.0001	0.000000000065736	0.00000000094358i

6. Discussion

Different NHSEs are solved by the HWCM proposed in this paper for different time and space intervals. The real and imaginary part of the numerical solution are compared with the exact solution in Figure 1, Figure 2 and with the Galerkin method in Table 4, where the same order of accuracy has been obtained for a lesser number of collocation points than the Galerkin method. In the theorem it is proved that the proposed method is second order accurate in space discretization, which is supported by the numerical results and verified by calculating the experimental rate of convergence (see Tables 1 and 5). The various results obtained by the proposed methods are compared with exact solutions as well as other existing methods. The propagation of soliton wave towards boundary from the origin is clearly shown in Figure 3 at a different final time, which is the important part while studying the Schrödinger equation. The conservation laws for energy and mass are preserved in Tables 2, 3, 6 and 7. The experimental rate of convergence and the maximum absolute errors are displayed in Tables 1 and 5. A comparison of HWCM is performed with other well known methods in Table 4 for a linear case and in Figure 4 for a nonlinear challenging case as well, which shows better performance of the HWCM.

Table 4. Comparison of different methods at $\Delta\tau = 0.001$ and $T = \pi^2$ for Test Problem 1.

HWCM			Galerkin Method (p^0) [11]			Galerkin Method (p^1) [11]	
$N = 2M$	E_∞^{Re}	E_∞^{Im}	N	E_∞^{Re}	E_∞^{Im}	E_∞^{Re}	E_∞^{Im}
16	2.38×10^{-2}	2.16×10^{-2}	20	2.09×10^{-1}	2.09×10^{-1}	3.79×10^{-2}	3.79×10^{-2}
32	4.21×10^{-3}	8.95×10^{-3}	40	8.69×10^{-2}	8.69×10^{-2}	5.05×10^{-3}	5.05×10^{-3}
64	1.73×10^{-3}	5.81×10^{-3}	80	4.11×10^{-2}	4.11×10^{-2}	1.31×10^{-3}	1.31×10^{-3}

Table 5. The numerical results at $\Delta\tau = 0.0001$, and $T = 1$ for Test Problem 2. Theoretical rate of convergence is 2 (see Theorem 1).

M	E_∞	Experimental Rate of Convergence
1	9.9872×10^{-2}	-
2	2.9424×10^{-2}	1.7630
4	7.9739×10^{-3}	1.8836
8	1.9021×10^{-3}	2.0676
16	4.7361×10^{-4}	2.0058

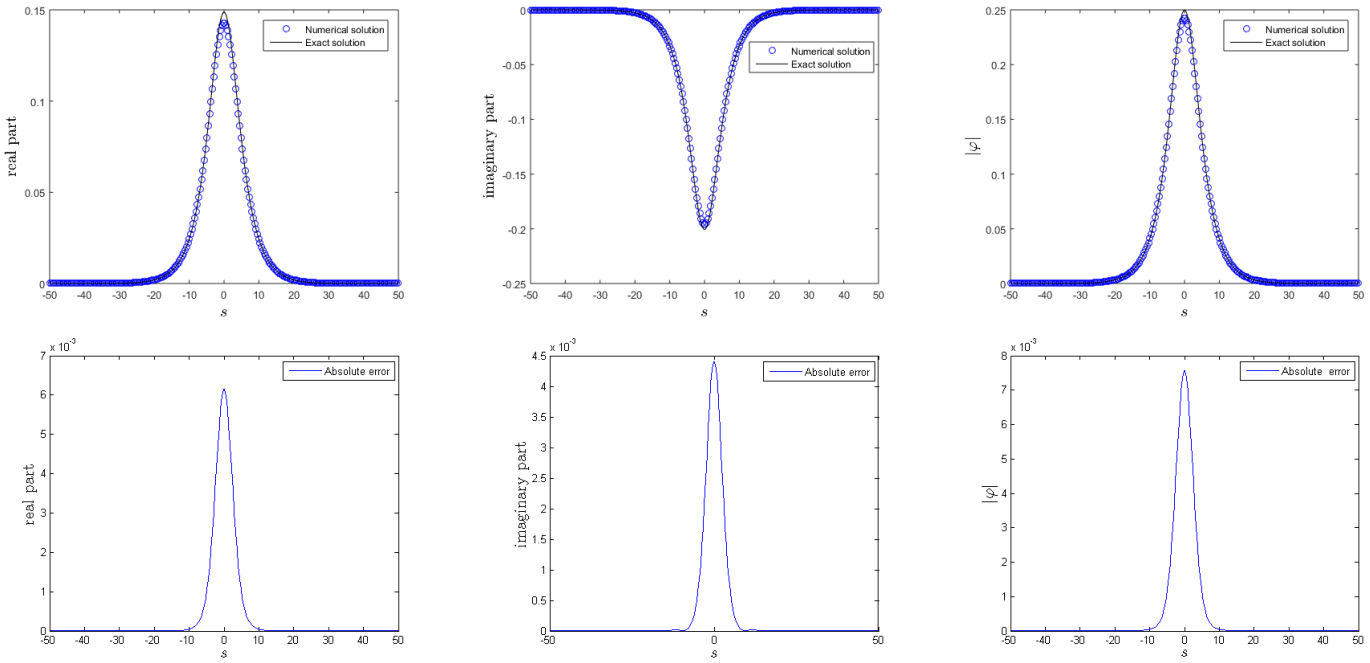

Figure 1. The solution and the absolute error at $M = 128$, $T = 1$ and $\Delta\tau = 0.001$ for Test Problem 2.

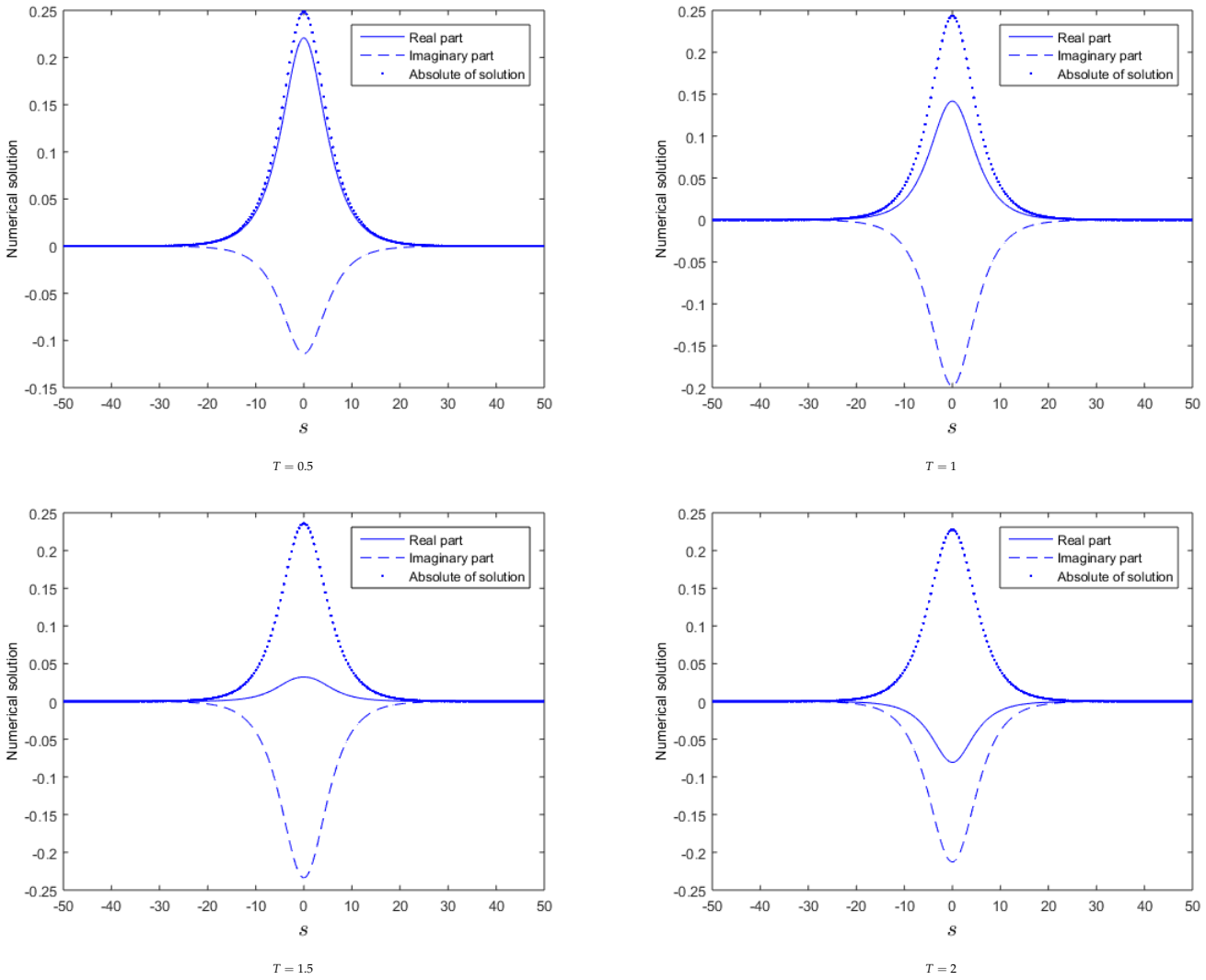

Figure 2. Profile of the numerical solutions at $M = 128$ and $\Delta\tau = 0.01$ with different T for Test Problem 2.

Table 6. Error norms and conservation laws at various time level with $M = 128$ and $\Delta\tau = 0.001$ for Test Problem 1.

T	E_{∞}^{Re}	E_{∞}^{Im}	E_{∞}	$\mathcal{E}$	$\mathcal{Q}$
0.1	9.8864×10^{-4}	1.0506×10^{-3}	1.0541×10^{-3}	2.249906963054199	1.999664635386422i
0.2	9.5558×10^{-4}	9.9005×10^{-4}	9.9772×10^{-4}	2.249936145461749	1.999568078806202i
0.3	9.0241×10^{-4}	9.5549×10^{-4}	9.7158×10^{-4}	2.249924837045404	1.999483611315301i
0.4	8.3248×10^{-4}	8.9079×10^{-4}	9.0917×10^{-4}	2.249851076414263	1.999387185040249i
0.5	7.5063×10^{-4}	7.9955×10^{-4}	8.1870×10^{-4}	2.249705208726114	1.999267565085404i
0.6	7.9987×10^{-4}	7.1485×10^{-4}	9.7909×10^{-4}	2.249488431902245	1.999123715667415i
0.7	8.3409×10^{-4}	7.6764×10^{-4}	1.1246×10^{-3}	2.249209466191778	1.998958893217779i
0.8	8.2634×10^{-4}	9.4861×10^{-4}	1.2538×10^{-3}	2.248882302999423	1.998777677883512i
0.9	7.7745×10^{-4}	1.1220×10^{-3}	1.3646×10^{-3}	2.248524815729122	1.998585531996365i
1	7.0575×10^{-4}	1.2804×10^{-3}	1.4550×10^{-3}	2.248157302414185	1.998388782032106i

Table 7. Error norms and conservation laws at various M with $T = 1$ and $\Delta\tau = 0.01$ for Test Problem 2.

M	E_{∞}^{Re}	E_{∞}^{Im}	E_{∞}	$\mathcal{E}$	$\mathcal{Q}$
8	4.5530×10^{-3}	1.5323×10^{-3}	4.8039×10^{-3}	0.000948069171383	0.000232841089347i
16	6.0002×10^{-3}	2.2329×10^{-3}	6.4022×10^{-3}	0.000985139322483	0.000254685053319i
32	6.7727×10^{-3}	2.7085×10^{-3}	7.2942×10^{-3}	0.000991057419645	0.000255807453310i
64	6.9416×10^{-3}	2.8066×10^{-3}	7.4875×10^{-3}	0.000992332262253	0.000256101948732i
128	6.9769×10^{-3}	2.8255×10^{-3}	7.5273×10^{-3}	0.000992632417626	0.000256178051069i
256	6.9852×10^{-3}	2.8299×10^{-3}	7.5367×10^{-3}	0.000992706293238	0.000256197214486i
512	6.9872×10^{-3}	2.8309×10^{-3}	7.5390×10^{-3}	0.000992724689529	0.000256202013479i

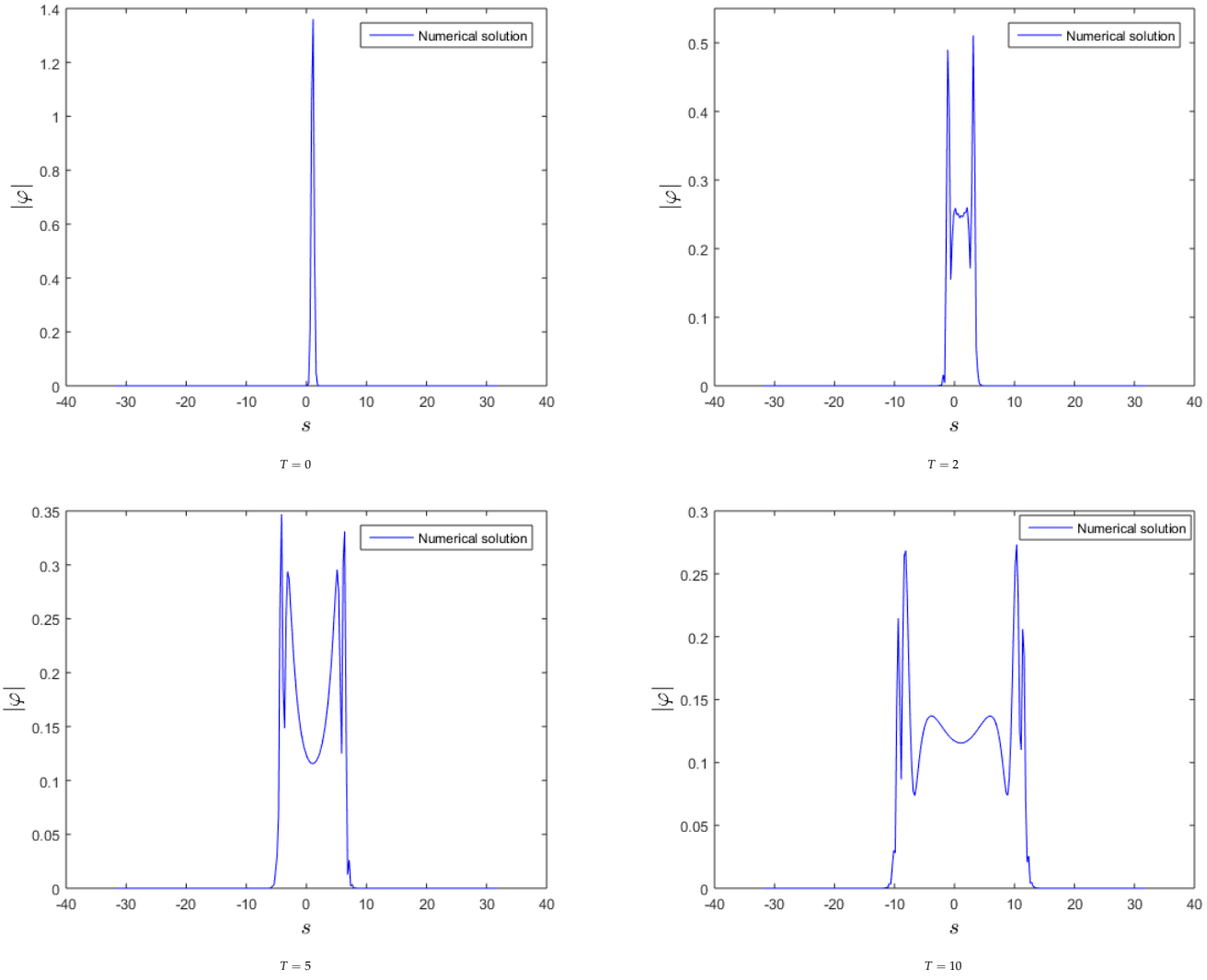

Figure 3. *Cont.*

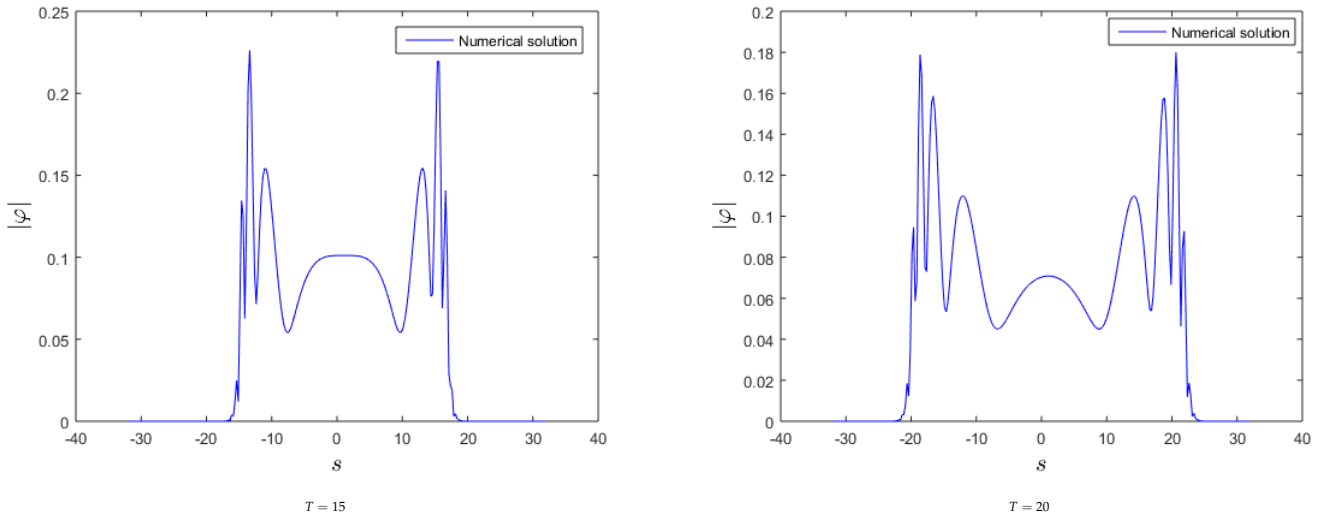

Figure 3. The profile of soliton wave at various T with $M = 128$ and $\Delta\tau = 0.01$ for Test Problem 3.

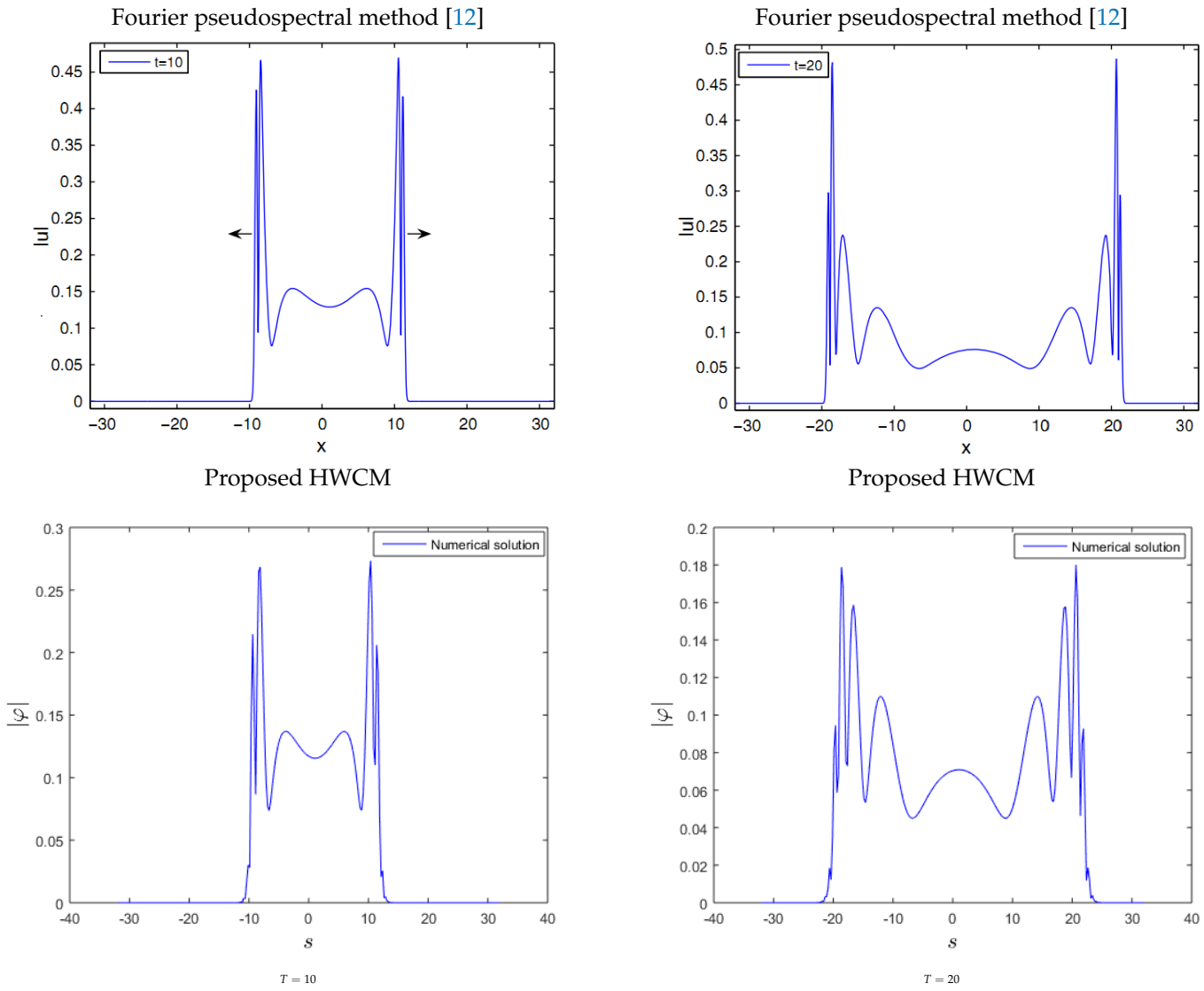

Figure 4. Comparison of propagating soliton obtained form different methods for Test Problem 3.

7. Conclusions

In this work, we have proposed the HWCM for the numerical solution of second-order NHSEs with wave operator. In different figures, it is shown that the propagating soliton waves are accurately captured by the proposed method and the HWCM has also been used to solve nonlinear problems with the blowup phenomena. The proposed HWCM preserves the energy as well as the mass, which have been highlighted for various examples. In different tables, the experimental rate of convergence is in line with the theoretical rate of convergence. The L_∞ error norm and the rate of convergence show that the proposed numerical method is accurate and applicable to solve NHSEs. Through the implementation of HWCM on different types of nonlinear equations and based on the above numerical experiments, we may conclude that the proposed HWCM is practical, time-efficient, and effective for solving NHSEs numerically. Due to the high potential achievements of the HWCM, the current scheme can be implemented to 2D and coupled NHSEs. These topics are the focus of our forthcoming work.

Author Contributions: Conceptualization, M.A. (Muhammad Ahsan) and M.A. (Masood Ahmad); methodology, M.A. (Muhammad Ahsan), M.N. and M.A. (Masood Ahmad); software, I.A. and H.A.; validation, M.A. (Muhammad Ahsan), X.L. (Xiaoling Liu) and X.L. (Xuan Liu); formal analysis, M.A. (Muhammad Ahsan) and I.A.; investigation, H.A. and M.A. (Masood Ahmad); resources, X.L. (Xiaoling Liu) and X.L. (Xuan Liu); data curation, M.A. (Masood Ahmad) and M.A. (Muhammad Ahsan); writing—original draft preparation, M.A. (Muhammad Ahsan); writing—review and editing, M.A. (Muhammad Ahsan) and I.A.; visualization, M.A. (Masood Ahmad), H.A. and M.N.; supervision, M.A. (Masood Ahmad); project administration, X.L. (Xiaoling Liu) and X.L. (Xuan Liu); funding acquisition, X.L. (Xiaoling Liu). All authors have read and agreed to the published version of the manuscript.

Funding: This research was supported by Characteristic innovation project of Guangdong Provincial Department of Education under No. 2017KTSCX124.

Institutional Review Board Statement: Not applicable.

Informed Consent Statement: Not applicable.

Data Availability Statement: Not applicable.

Acknowledgments: We wish to acknowledge the anonymous referees whose suggestions have helped improve the quality of our paper.

Conflicts of Interest: The authors declare no conflict of interest.

Nomenclature

ODEs	ordinary differential equations
PDEs	partial differential equation equations
NHSEs	nonlinear hyperbolic Schrödinger equations
HWCM	Haar wavelet collocation method
φ	unknown complex function
s	space variable
τ	time variable
$\mathcal{E}(\tau)$	energy invariant
$\mathcal{Q}(\tau)$	mass invariant
$\overline{w}_0(\tau)$	function of variable τ
$\widetilde{w}_0(s,\tau)$	function of variables τ and s
μ_i	constant parameter, where $i = 1, 2, 3, 4$ and 5
$h_i(s)$	Haar wavelet function
$a, \zeta_1, \zeta_2, \zeta_3$ and b	some real numbers
$p_{i,1}(s)$	integral of $h_i(s)$ from a to s
$p_{i,2}(s)$	integral of $p_{i,1}(s)$ from a to s
C	integral of $p_{i,1}(s)$ from a to b
λ_i	unknown Haar wavelet coefficients

i	$\sqrt{-1}$
2M	number of collocation points
s_l	collocation points
$\Delta\tau$	time discretisizing unit
I_1, I_2, B_1 and B_2	given known functions
$L_\infty(a,b)$	infinity-norm in the interval (a,b)
$\varphi_M(s,\tau)$	Haar wavelet representation of φ
$\widetilde{\varphi}_M^{n+1}(s)$	approximate numerical value of φ
$E_M(s,\tau)$	error term due to Haar wavelet approximation
$\mathcal{E}_{\mathcal{M}}^{\mathcal{H}}(s,\tau)$	Haar wavelet truncation error term
$\mathcal{O}(\Delta\tau^2)$	truncation error due to time discretization
P	positive integer
p	all positive integer up to P
Re	real part
Im	imaginary part
E_∞	infinity error
E_∞^{Re}	maximum absolute error of real part
E_∞^{Im}	maximum absolute error of imaginary part

References

1. Wang, L.; Kong, L.; Zhang, L.; Zhou, W.; Zheng, X. Multi-symplectic preserving integrator for the Schrödinger equation with wave operator. *Appl. Math. Model.* **2015**, *39*, 6817–6829. [CrossRef]
2. Bergé, L.; Colin, T. A singular perturbation problem for an envelope equation in plasma physics. *Phys. D Nonlinear Phenom.* **1995**, *84*, 437–459. [CrossRef]
3. Bao, W.; Dong, X.; Xin, J. Comparisons between sine-Gordon and perturbed nonlinear Schrödinger equations for modeling light bullets beyond critical collapse. *Phys. D Nonlinear Phenom.* **2010**, *239*, 1120–1134. [CrossRef]
4. Machihara, S.; Nakanishi, K.; Ozawa, T. Nonrelativistic limit in the energy space for nonlinear Klein-Gordon equations. *Math. Ann.* **2002**, *322*, 603–621. [CrossRef]
5. Guo, B.; Li, H. On the problem of numerical calculation for a class of the system of nonlinear Schrödinger equations with wave operator. *J. Numer. Methods Comput. Appl.* **1983**, *4*, 258–263.
6. Fei, Z.; Pérez-García, V.M.; Vázquez, L. Numerical simulation of nonlinear Schrödinger systems: A new conservative scheme. *Appl. Math. Comput.* **1995**, *71*, 165–177. [CrossRef]
7. Wang, T.C.; Zhang, L.M. Analysis of some new conservative schemes for nonlinear Schrödinger equation with wave operator. *Appl. Math. Comput.* **2006**, *182*, 1780–1794. [CrossRef]
8. Li, X.; Zhang, L.; Zhang, T. A new numerical scheme for the nonlinear Schrödinger equation with wave operator. *J. Appl. Math. Comput.* **2017**, *54*, 109–125. [CrossRef]
9. Wang, T.; Guo, B. Unconditional convergence of two conservative compact difference schemes for non-linear Schrödinger equation in one dimension. *Sci. Sin. Math.* **2011**, *41*, 207–233. [CrossRef]
10. Wang, S.; Zhang, L.; Fan, R. Discrete-time orthogonal spline collocation methods for the nonlinear Schrödinger equation with wave operator. *J. Comput. Appl. Math.* **2011**, *235*, 1993–2005. [CrossRef]
11. Guo, L.; Xu, Y. Energy conserving local discontinuous Galerkin methods for the nonlinear Schrödinger equation with wave operator. *J. Sci. Comput.* **2015**, *65*, 622–647. [CrossRef]
12. Ji, B.; Zhang, L. An exponential wave integrator Fourier pseudospectral method for the nonlinear Schrödinger equation with wave operator. *J. Appl. Math. Comput.* **2018**, *58*, 273–288. [CrossRef]
13. Jin, Q.; Wang, W. Analysis of the iteratively regularized Gauss–Newton method under a heuristic rule. *Inverse Problems* **2018**, *34*, 1–24. [CrossRef]
14. Jin, Q. On a heuristic stopping rule for the regularization of inverse problems by the augmented Lagrangian method. *Numer. Math.* **2017**, *136*, 973–992. [CrossRef]
15. Jin, Q.; Lu, X. A fast nonstationary iterative method with convex penalty for inverse problems in Hilbert spaces. *Inverse Problems* **2014**, *30*, 1–21. [CrossRef]
16. Liu, Y.; Liu, Y.; Cen, Z. Daubechies wavelet meshless method for 2-D elastic problems. *Tsinghua Sci. Technol.* **2008**, *13*, 605–608. [CrossRef]
17. Díaz, L.A.; Martín, M.T.; Vampa, V. Daubechies wavelet beam and plate finite elements. *Finite Elem. Anal. Des.* **2009**, *45*, 200–209. [CrossRef]
18. Jang, G.W.; Kim, Y.; Choi, K. Remesh-free shape optimization using the wavelet-Galerkin method. *Int. J. Solids Struct.* **2004**, *41*, 6465–6483. [CrossRef]

19. Siraj-ul-Islam; Aziz, I.; Al-Fhaid, A.S. An improved method based on Haar wavelets for numerical solution of nonlinear integral and integro-differential equations of first and higher orders. *J. Comput. Appl. Math.* **2014**, *260*, 449–469. [CrossRef]
20. Ahsan, M.; Ahmad, I.; Ahmad, M.; Hussian, I. A numerical Haar wavelet-finite difference hybrid method for linear and non-linear Schrödinger equation. *Math. Comput. Simul.* **2019**, *165*, 13–25. [CrossRef]
21. Dahmen, W.; Kurdila, A.J.; Oswald, P. (Eds.) *Multiscale Wavelet Methods for Partial Differential Equations*; Wavelet Analysis and Its Applications; Academic Press, Inc.: San Diego, CA, USA, 1997; Volume 6, pp. xiv+570.
22. Tran, T.; Stephan, E.P.; Mund, P. Hierarchical basis preconditioners for first kind integral equations. *Appl. Anal.* **1997**, *65*, 353–372. [CrossRef]
23. Maleknejad, K.; Mirzaee, F. Using rationalized Haar wavelet for solving linear integral equations. *Appl. Math. Comput.* **2005**, *160*, 579–587. [CrossRef]
24. Lepik, U. Haar wavelet method for nonlinear integro-differential equations. *Appl. Math. Comput.* **2006**, *176*, 324–333. [CrossRef]
25. Lepik, U. Numerical solution of evolution equations by the Haar wavelet method. *Appl. Math. Comput.* **2007**, *185*, 695–704. [CrossRef]
26. Hsiao, C.H. Haar wavelet approach to linear stiff systems. *Math. Comput. Simul.* **2004**, *64*, 561–567. [CrossRef]
27. Hsiao, C.H.; Wang, W.J. Haar wavelet approach to nonlinear stiff systems. *Math. Comput. Simul.* **2001**, *57*, 347–353. [CrossRef]
28. Shah, F.A.; Abass, R.; Iqbal, J. Numerical solution of singularly perturbed problems using Haar wavelet collocation method. *Cogent Math.* **2016**, *3*, 1202504. [CrossRef]
29. Shah, F.A.; Abass, R. An operational Haar wavelet collocation method for solving singularly perturbed boundary-value problems. *SeMA J.* **2017**, *74*, 457–474. [CrossRef]
30. Aziz, I.; Amin, R. Numerical solution of a class of delay differential and delay partial differential equations via Haar wavelet. *Appl. Math. Model.* **2016**, *40*, 10286–10299. [CrossRef]
31. Aziz, I.; Siraj-ul-Islam; Khan, F. A new method based on Haar wavelet for the numerical solution of two-dimensional nonlinear integral equations. *J. Comput. Appl. Math.* **2014**, *272*, 70–80. [CrossRef]
32. Siraj-ul-Islam; Aziz, I.; Haq, F. A comparative study of numerical integration based on Haar wavelets and hybrid functions. *Comput. Math. Appl.* **2010**, *59*, 2026–2036. [CrossRef]
33. Aziz, I.; Siraj-ul-Islam; Šarler, B. Wavelets collocation methods for the numerical solution of elliptic BV problems. *Appl. Math. Model.* **2013**, *37*, 676–694. [CrossRef]
34. Jiwari, R. A Haar wavelet quasilinearization approach for numerical simulation of Burgers' equation. *Comput. Phys. Commun.* **2012**, *183*, 2413–2423. [CrossRef]
35. Siraj-ul-Islam; Aziz, I.; Ahmad, M. Numerical solution of two-dimensional elliptic PDEs with nonlocal boundary conditions. *Comput. Math. Appl.* **2015**, *69*, 180–205. [CrossRef]
36. Ahsan, M.; Siraj-ul-Islam; Hussain, I. Haar wavelets multi-resolution collocation analysis of unsteady inverse heat problems. *Inverse Probl. Sci. Eng.* **2019**, *27*, 1498–1520. [CrossRef]
37. Siraj-ul-Islam; Ahsan, M.; Hussian, I. A multi-resolution collocation procedure for time-dependent inverse heat problems. *Int. J. Therm. Sci.* **2018**, *128*, 160–174. [CrossRef]
38. Majak, J.; Shvartsman, B.; Pohlak, M.; Karjust, K.; Eerme, M.; Tungel, E. Solution of fractional order differential equation by the Haar wavelet method. Numerical convergence analysis for most commonly used approach. In Proceedings of the AIP Conference Proceedings, Chania, Greece, 6–11 June 2016; AIP Publishing LLC: Melville, NY, USA, 2016; Volume 1738, p. 480110.
39. Li, Y.; Zhao, W. Haar wavelet operational matrix of fractional order integration and its applications in solving the fractional order differential equations. *Appl. Math. Comput.* **2010**, *216*, 2276–2285. [CrossRef]
40. Yi, M.; Huang, J. Wavelet operational matrix method for solving fractional differential equations with variable coefficients. *Appl. Math. Comput.* **2014**, *230*, 383–394. [CrossRef]
41. Saeed, U.; ur Rehman, M. Haar wavelet Picard method for fractional nonlinear partial differential equations. *Appl. Math. Comput.* **2015**, *264*, 310–322. [CrossRef]
42. Wang, L.; Ma, Y.; Meng, Z. Haar wavelet method for solving fractional partial differential equations numerically. *Appl. Math. Comput.* **2014**, *227*, 66–76. [CrossRef]
43. Nazir, S.; Shahzad, S.; Wirza, R.; Amin, R.; Ahsan, M.; Mukhtar, N.; García-Magariño, I.; Lloret, J. Birthmark based identification of software piracy using Haar wavelet. *Math. Comput. Simul.* **2019**, *166*, 144–154. [CrossRef]
44. Hariharan, G.; Kannan, K.; Sharma, K. Haar wavelet method for solving Fisher's equation. *Appl. Math. Comput.* **2009**, *211*, 284–292. [CrossRef]
45. Talukder, K.H.; Harada, K. Haar wavelet based approach for image compression and quality assessment of compressed image. *arXiv* **2010**, arXiv:1010.4084.
46. Sarkar, S.; Bhairannawar, S.S. Efficient FPGA architecture of optimized Haar wavelet transform for image and video processing applications. *Multidimens. Syst. Signal Process.* **2021**, *32*, 821–844. [CrossRef]
47. Aznam, S.M.; Chowdhury, M. Generalized Haar wavelet operational matrix method for solving hyperbolic heat conduction in thin surface layers. *Results Phys.* **2018**, *11*, 243–252. [CrossRef]
48. Pandit, S.; Jiwari, R.; Bedi, K.; Koksal, M.E. Haar wavelets operational matrix based algorithm for computational modelling of hyperbolic type wave equations. *Eng. Comput.* **2017**, *34*, 2793–2814. [CrossRef]

49. Pervaiz, N.; Aziz, I. Haar wavelet approximation for the solution of cubic nonlinear Schrodinger equations. *Phys. A Stat. Mech. Its Appl.* **2020**, *545*, 1–17. [CrossRef]
50. Liu, X.; Ahsan, M.; Ahmad, M.; Hussian, I.; Alqarni, M.; Mahmoud, E. Haar wavelets multi-resolution collocation procedures for two-dimensional nonlinear Schrödinger equation. *Alex. Eng. J.* **2021**, *60*, 3057–3071. [CrossRef]
51. Majak, J.; Shvartsman, B.; Kirs, M.; Pohlak, M.; Herranen, H. Convergence theorem for the Haar wavelet based discretization method. *Compos. Struct.* **2015**, *126*, 227–232. [CrossRef]